Protein Science (1994), *3*:2023–2032. Cambridge University Press. Printed in the USA.

Engineering the quaternary structure of an enzyme: Construction and analysis of a monomeric form of malate dehydrogenase from *Escherichia coli*

DEBORAH R. BREITER, ERNESTO RESNIK, AND LEONARD J. BANASZAK
Department of Biochemistry, University of Minnesota, Minneapolis, Minnesota 55455

(RECEIVED June 14, 1994; ACCEPTED August 30, 1994)

Abstract

The citric acid cycle enzyme, malate dehydrogenase (MDH), is a dimer of identical subunits. In the crystal structures of 2 prokaryotic and 2 eukaryotic forms, the subunit interface is conformationally homologous. To determine whether or not the quaternary structure of MDH is linked to the catalytic activity, mutant forms of the enzyme from *Escherichia coli* have been constructed. Utilizing the high-resolution structure of *E. coli* MDH, the dimer interface was analyzed critically for side chains that were spatially constricted and needed for electrostatic interactions. Two such residues were found, D45 and S226. At their nearest point in the homodimer, they are in different subunits, hydrogen bond across the interface, and do not interact with any catalytic residues. Each residue was mutated to a tyrosine, which should disrupt the interface because of its large size. All mutants were cloned and purified to homogeneity from an *mdh*$^-$ *E. coli* strain (BHB111). Gel filtration of the mutants show that D45Y and D45Y/S226Y are both monomers, whereas the S226Y mutant remains a dimer. The monomeric D45Y and D45Y/S226Y mutants have 14,000- and 17,500-fold less specific activity, respectively, than the native enzyme. The dimeric S226Y has only 1.4-fold less specific activity. All forms crystallized, indicating they were not random coils. Data have been collected to 2.8 Å resolution for the D45Y mutant. The mutant is not isomorphous with the native protein and work is underway to solve the structure by molecular replacement.

Keywords: dimer interface; malate dehydrogenase; *mdh*$^-$ *E. coli* strain; monomeric MDH; site-directed mutagenesis; subunit dissociation

Malate dehydrogenase is an enzyme that plays an important role in the citric acid cycle. The MDHs utilize the cofactor NAD to catalyze the reversible oxidation of malate to oxaloacetate. In the direction of oxaloacetate production, the reactants are NAD and malate, the dicarboxylic acid, and the products are NADH, oxaloacetate, and a proton. All known MDHs are active as dimers of identical subunits. In oligomeric enzymes, the role the subunit interface plays in catalytic activity has been controversial. However, a clear interface dependence in MDH is demonstrated by the mutational studies described below.

The design of the mutants was based on 4 different crystal structures of MDHs. Two eukaryotic MDHs, isolated from both the cytoplasm and mitochondria of pig heart, have known 3-dimensional structures and similar subunit–subunit interfaces (Roderick & Banaszak, 1986; Birktoft et al., 1989; Gleason et al., 1994). In addition, crystal structures of 2 prokaryotic MDHs from *Escherichia coli* and *Thermus flavus* have been solved and also have homologous active sites and quaternary structures (Hall et al., 1992; Kelly et al., 1993).

A comparison of the overall conformation, active sites, and subunit interfaces of all the MDHs demonstrated a high degree of structural similarity, which exists in spite of a sometimes low amino acid sequence identity between forms. For example, the mMDH and cMDH from pig heart are only 20% identical. However, eMDH has 58% sequence identity with pig heart mMDH, but only about 20% identity with pig heart cMDH (Hall et al., 1992; Gleason et al., 1994). The prokaryotic forms

Reprint requests to: Leonard J. Banaszak, Department of Biochemistry, 4-225 Millard, University of Minnesota, 435 Delaware Street S.E., Minneapolis, Minnesota 55455; e-mail: len_b@dccc.med.umn.edu.

Abbreviations: MDH, malate dehydrogenase; mMDH, MDH from the mitochondria; cMDH, MDH from the cytosol; eMDH, MDH from *Escherichia coli*; *mdh*, the gene that encodes MDH; LDH, lactate dehydrogenase; TIM, triosephosphate isomerase; Amp, ampicillin; Kan, kanamycin; Strep, streptomycin; Tet, tetracycline; ^{R}, resistance; ^{S}, sensitivity; *kan*, gene encoding Kan^R; Tn; transposon; Tn*10*, gene encoding Tet^R; Hfr, high-frequency chromosome transfer; P1, P1 bacteriophage; PEG, polyethylene glycol; PEI, polyethyleneimine; T, total acrylamide; DTT, dithiothreitol; IPTG, isopropyl β-D-thioglucopyranoside; C, percent crosslinked; Hepes, 4-(2-hydroxyethyl)-1-piperazineethanesulfonic acid; MOPS, 3-(*N*-morpholino)propanesulfonic acid.

of MDH are usually homologous with the mitochondrial MDH. However, one known exception is the MDH isolated from *T. flavus*, which is homologous with cMDH (Honka et al., 1990).

Crystallographic studies have shown that the dimer interface consists mainly of interacting α-helices that fit compactly together. The active sites in these dimeric proteins are well separated from each other; they are not in the subunit interface and the bound dicarboxylic acid substrates are separated by about 30 Å. The 3-dimensional subunit-subunit relationship is the same in all of the known MDH structures and in one of the interfaces present in the tetrameric lactate dehydrogenases.

The oligomeric structure of MDH has a variety of biological implications. Some researchers have suggested the dimer structure is critical for enzymatic activity. Our studies concerning the catalytic mechanism of eMDH utilize site-directed mutagenesis to establish the significance of the subunit interface. The first goal was to construct and characterize a stable monomer. Several highly conserved amino acid residues are found in this interface (Fig. 1), with D45 and H48 having the most extensive hydrogen bonding interactions. We were uncertain from the start as to whether or not mutating MDH to a monomeric form would have a significant effect on catalytic activity. Much research has been done toward understanding how the interactions between subunits contribute toward the kinetics and the catalytic mechanism, and the direct involvement of the subunit interface in the dimeric MDHs has been controversial.

Two schools of thought arose surrounding the structure-function relationship. Harada and Wolfe (1968) first proposed the reciprocating compulsory ordered mechanism where each subunit alternates as the "active" and the "helper" subunit, but both are needed for activity. This mechanism predicts an inactive monomer, and was corroborated by studies that showed a dramatic reduction of enzymatic activity on dissociation to monomers at low enzyme concentration, at pH 5.0, and in the absence of substrates (Bleile et al., 1977; Wood et al., 1981a, 1981b). The second mechanism (Mullinax et al., 1982) introduces an equilibrium between 2 conformers of MDH, one of which preferentially binds citrate and NAD^+, whereas the other binds NADH. This would suggest an active monomer. Evidence for this idea is exhibited by an immobilized monomeric form of MDH (Jurgensen et al., 1981; DuVal et al., 1985), and a hybrid-modified form of MDH (Jurgensen & Harrison, 1982; McEvily et al., 1985) having some catalytic function. The definitive answer appears to hinge on the question of whether a stable monomer can be isolated and whether it has activity.

Previous mutagenesis studies have been completed on the dimer interface of the mitochondrial form of MDH from *Saccharomyces cerevisiae* (Steffan & McAlister-Henn, 1991). Two of the highly conserved residues at the interface, D43 and H46 (D45 and H48 eMDH numbering; see Fig. 1) were mutated. The H46L mutation resulted in an enzyme that had an optimal activity pH of 5.5 and was even more active than the native enzyme. The pH optimum for the native enzyme is 7.5. Gel-filtration results of the H46L mutant suggest that this mutant enzyme is a dimer, even at pH 5.0, where the native enzyme would be a monomer. This shift in optimal pH and increase in activity seemed to correspond with an increase in the stability of the dimer. Because H46L does not undergo the pH-induced dissociation, H46 could be one of the amino acid residues responsible for the formation of inactive monomers at pH 5.0, at least for the pig heart mMDH (Bleile et al., 1977). At low pH, H46 would undergo protonation resulting in the dissociation of the dimeric enzyme and reduced activity. The D43N mutation resulted in an essentially inactive enzyme, which gel filtration suggests is extensively denatured. Unfortunately, in this study a stable monomer was not obtained.

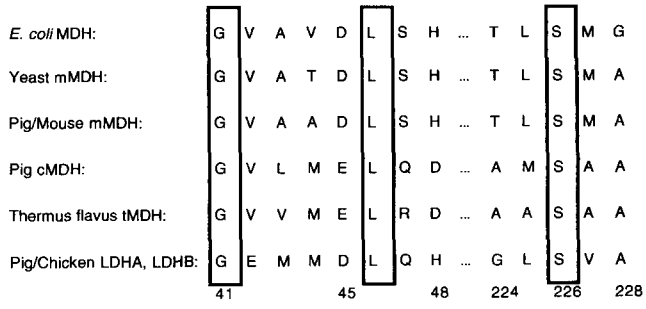

Fig. 1. Homology within a portion of the α-helical region in the dimer interface. In *E. coli* MDH, D45 and H48 have the most extensive hydrogen bonding pattern (Hall et al., 1992). Residue numbers correspond to *E. coli* MDH.

A successful study involving mutagenesis of a dimeric protein to a monomeric protein was accomplished by Borchert et al. (1993) with triosephosphate isomerase. A monomeric form of TIM was constructed by replacing a 15-residue loop, which contained most of the subunit-subunit interactions, with an 8-residue fragment. The "monoTIM" has 0.1% of the catalytic activity of wild-type TIM, with a k_{cat} value 1,000-fold lower and a K_m value 20-fold higher than the wild-type enzyme. They speculate that the second subunit positions the catalytic residues correctly and loss of activity is a result of the incorrect positioning of the catalytic residues K13 and H95.

Other workers have prepared a dimeric form of the normally tetrameric LDH using mutagenesis (Jackson et al., 1992). The mutant dimeric form of LDH probably resembles the MDHs because the mutation replaces a surface loop on LDH near the P-interface with the larger loop found in the MDHs. The P-interface is special to the tetrameric LDHs; the Q-interface is the one present in both LDH and MDH, and it is one that is altered in the studies to be described below.

With the high-resolution structural data resulting from the crystallographic studies of eMDH (Hall et al., 1992), we felt it would be possible to identify a single site that would lead to dimer dissociation. If a monomeric form of MDH was obtainable, then such mutant proteins could be used to test the theory that catalysis is dependent on the oligomeric state of the MDH molecule. Although the crystallographic model does not suggest a direct link between the active site and the subunit interface, indirect connections are present. Briefly, H48 at the subunit interface is within hydrogen bonding distance of R153 of the other subunit. This is 1 of 3 arginine side chains (R153, R81, and R87) that are involved in the binding of the dicarboxylic acid substrates (Hall et al., 1992). Overall, the interface region near H48 includes a number of cationic side chains. Amid these basic residues is a spatially constricted acidic side chain, D45, which is within hydrogen bonding distance of S226, T224, and K217, in another subunit. The targets for mutagenesis, with the goal being a stable monomer, were D45 and S226, which interact across the dimer interface and have no direct interactions with any catalytic residues.

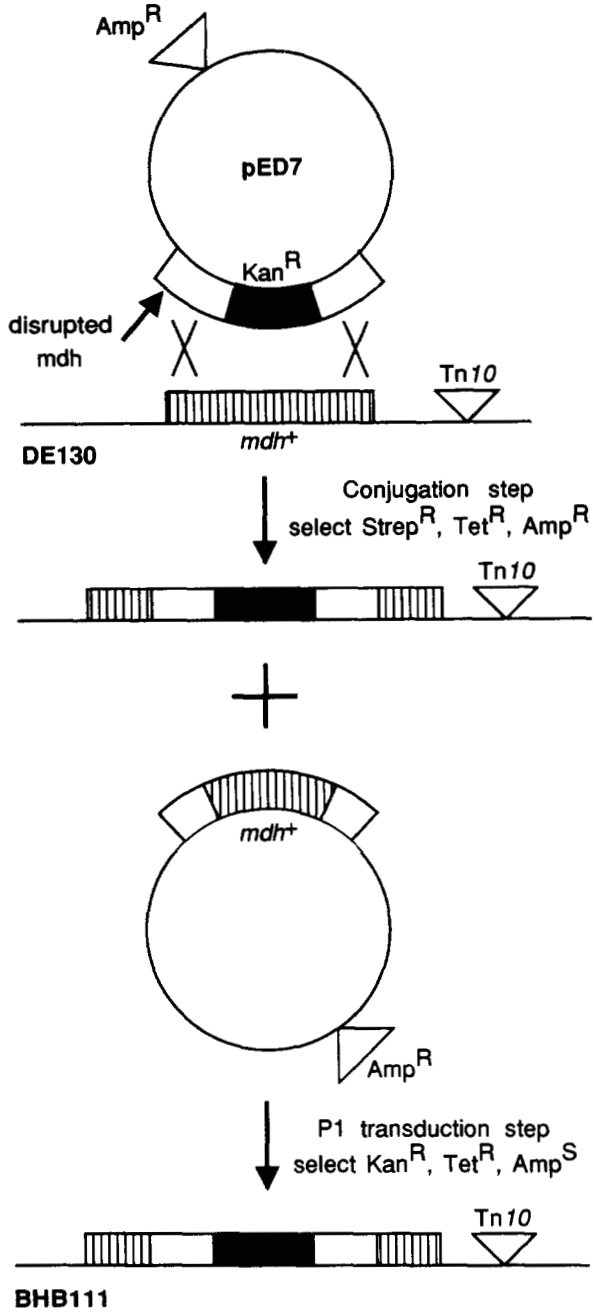

Fig. 2. Construction of BHB111. The plasmid pED7 carrying the Kan^R disrupted *mdh* gene is shown in the topmost part of the diagram along with the Hfr donor strain DE130. Strain DE130 was transformed with pED7 and homologous recombination occurs between the sequences flanking the *kan* gene. After conjugation with an F$^-$ recipient strain, the culture is grown in a medium that contains the appropriate antibiotics to select for exconjugates that have the *kan* gene disrupting the chromosome. We use Amp to select for recipients with the plasmid, Kan for the disruption, Tet to ensure inheritance of the Tn*10* gene, and Strep to select against the donor. The recipient strain is Strep^R. The desired strain is identified and a P1 transduction is done to insert the sequences into the same recipient strain, now without the plasmid. Transductants can be tested for Amp^S to ensure they have not inherited the original plasmid. The desired product (BHB111) was analyzed thoroughly for correct antibiotic selection, growth conditions, lack of enzymatic activity, and frequency of cotransduction of antibiotic markers. The indicated Tn*10* exhibits 26% cotransduction with *kan*. Straight lines indicate chromosomal sequences and plasmids are circular, and the representation is not drawn to scale.

Table 1. *E. coli strains and plasmids*

Strain or plasmid	Relevant genotype	Source
DV21A05	HFr, relA1, Δ(speC-glc)63, spot1, ppc-2, thi-1, aceB6	CGSC[a]
CAG12071	MG1655(wild-type), zhb::Tn10	C.A. Gross
DE130	DV21A05, zhb::Tn10	This study
W4680	F-, ΔlacZ39, rpsL, melB4	CGSC
BHB111	W4680, zhb::Tn10 mdh$^-$ (mdh-690::kan^R)	This study
pRV7	mdh gene	K.-D. Entian
pED7	pRV7, mdh-690::kan^R	This study
pT7/T3α-18	Phagemid suitable for mutagenesis, sequencing, and expression	Gibco BRL
pMBBα-18	pT7/T3α-18, mdh gene	This study

[a] CGSC: *E. coli* Genetic Stock Center, Yale University.

Results

Construction of an mdh$^-$ E. coli strain: BHB111

In order to simplify the purification of the site-directed mutants, an *mdh*$^-$ strain of *E. coli* (BHB111) was constructed. The strategy is shown schematically in Figure 2. Briefly, the chromosomal *mdh* gene was disrupted with a *kan* cassette. All of the strains and plasmids used are summarized in Table 1.

BHB111 was analyzed thoroughly for correct antibiotic selection, growth conditions, lack of enzymatic activity, and frequency of cotransduction of antibiotic markers. BHB111 had several markers for selection including resistance to Kan, Strep, Tet, and sensitivity to Amp. The new strain responded correctly to these markers. Furthermore, without MDH, much of the citric acid cycle is inoperable. Growth conditions were therefore examined and the results are shown in Table 2. BHB111 grows on MOPS-minimal media containing glucose but not acetate. This growth phenotype is typical for a disruption in the tricarboxylic acid cycle. As expected and is apparent in the data given in Table 2, the parent strain W4680 can grow on minimal media containing acetate. Although the *mdh*$^-$ strain grew somewhat slower than the parent, reasonable cell production was possible.

To compare the relative MDH activities of the BHB111 strain versus its parent strain (W4680), crude extracts from W4680, BHB111, and BHB111 with plasmid pMBBα-18 were prepared and analyzed. Plasmid pMBBα-18 contains the wild-type *mdh*

Table 2. *Doubling time of BHB111 versus W4680*[a]

Strain (carbon source)	Time (min)
BHB111 (acetate)	No growth
BHB111 (glucose)	114
W4680 (acetate)	123
W4680 (glucose)	90

[a] The strains were grown in MOPS-minimal media with 1% of either glucose or acetate. The error is about 10%.

gene. The MDH activities are given in Table 3. The results are striking. The crude extract from the wild-type strain or plasmid had activity and BHB111 had none. The apparent complete loss of MDH activity in extracts from the mutant strain corroborates the fact that BHB111 has a disrupted *mdh* gene.

The frequency of cotransduction of the Kan^R and Tet^R markers was also determined and related to the distance between the markers, to convince ourselves completely that we had constructed an *mdh*$^-$ strain. The Tn*10* gene is located near or at the *zhb* gene in DE130 × W4680 (the parent strain of BHB111), at about 69.7 min, and the *mdh* gene is at about 70 min. So, if the *kan* gene is located in the middle of the *mdh* gene, the distance between the 2 markers should be less than 1 min. The frequency of cotransduction was 26%. The determined distance between the markers is 0.72 min, which shows that the *kan* cassette could be integrated in the right position to disrupt production of wild-type MDH.

Site-directed mutagenesis of E. coli MDH

As noted above, 2 residues were selected as possible sites for producing monomeric mutants of eMDH, D45, and S226. Single-base substitutions were introduced to change both residues to tyrosines, from a GAT (D) or a TCT (S) to a TAT (Y). To date, 3 mutants of *E. coli* MDH have been constructed and confirmed by DNA sequencing, D45Y, S226Y, and the double mutant D45Y/S226Y. Not only did the sequencing confirm that the mutagenesis was successful, but a mistake in the original wild-type MDH sequence was found. There should be an alanine at position 80 not an arginine.

To compare structural and kinetic properties, the wild-type and mutant proteins were purified in parallel experiments. The native (pMBBα-18) and mutant plasmids were separately transformed into BHB111, the *mdh*$^-$ strain. All cells were grown in a high-density fermentor under the same conditions. Purification conditions were the same for all the mutants and the native MDH. A Q-Sepharose column was used initially, followed by chromatography on a Blue Sepharose column. On the Q-Sepharose column, the native and S226Y mutant behaved similarly, with much of the MDH activity eluting immediately from the column with some enzymatic activity appearing in the initial salt fractions. However, the D45Y and D45Y/S226Y mutants eluted in the initial breakthrough fractions. We emphasize that these are qualitative observations because the activity of both the D45Y and double mutant is very low, making it difficult to detect enzymatic activity.

The proteins also eluted differently on the Blue Sepharose column, with the native and double mutant eluting at about 200 mM NaCl, the S226Y mutant eluting at 270 mM NaCl, and the D45Y eluting at 130 mM NaCl. All mutants were purified to homogeneity on the Blue Sepharose column, as confirmed by SDS-PAGE. Purification of the D45Y and double mutant would have been difficult without the *mdh*$^-$ *E. coli* strain because of their low specific activities.

The purified proteins were characterized by several methods. An isoelectric focusing gel shows the pI of the native and S226Y protein to be 5.2. However, D45Y and D45Y/S226Y both have a somewhat higher pI of 5.85. On a 20% homogenous gel run under native conditions, the native and S226Y proteins co-migrated, as did the D45Y and double mutant.

Gel-filtration chromatography was utilized to determine the molecular weights of the different purified enzymes. The results are shown in Figure 3. The native protein and all 3 mutants were loaded on a Sephadex G-200 column at a pH of 7.2. The elution profiles were examined by monitoring the OD at 280 nm and by MDH assays. Seven standards, all shown in Figure 3, were used to calibrate the column. Molecular weights of the different MDHs were determined from the retention time on the column. The wild-type enzyme produced an elution profile with an apparent molecular weight of 59,200, confirming a dimeric form of the enzyme. The S226Y mutant enzyme gave the same elution profile, and therefore is also a dimer. The D45Y and D45Y/S226Y mutants, however, had retention times corresponding to molecular weights of 32,600 and 31,400, respectively, indicating a properly folded monomeric form of MDH.

Because the goal of this research was to relate quaternary structure and the catalytic activity, the specific activities and V_{max} of the native versus the mutant enzymes along with the K_m for NAD and malate were determined and are tabulated in Table 4. As is apparent in Table 4, the 4 forms of MDH fell into

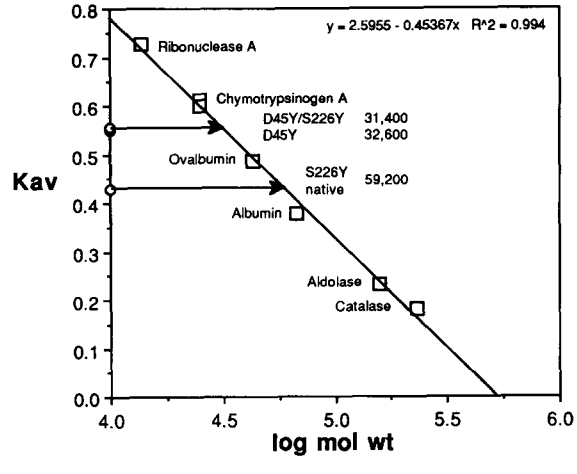

Fig. 3. Gel-filtration chromatography of purified wild-type and mutant forms of *E. coli* MDH. The chromatography was conducted using a Sephadex G-200 column equilibrated in pH 7.4 buffer at 4 °C. The calibration curve was determined using standards of known molecular weights. On the *x*-axis is the $\log_{10}$ of the molecular weight and on the *y*-axis is K_{av}, a combination of various elution parameters. $K_{av} = (V_e - V_0)/(V_t - V_0)$, where V_e is the elution volume for the protein, V_0 is the column void volume, and V_t is the total bed volume. The standards are small boxes that are labeled with the name of the protein. The K_{av}'s for native and mutant MDHs are indicated by a circle on the *y*-axis. An arrow points to the determined molecular weight for each protein.

Table 3. *MDH activity in crude extract of E. coli strains*[a]

Strain (plasmid)	Specific activity (units/mg)
W4680	7.2
BHB111	0.0
BHB111 (pMBBα-18)	15.1

[a] MDH activity was determined as described in the Materials and methods section. The protein concentration of the crude extract was determined by a Bio-Rad assay versus BSA.

Table 4. *MDH activity*[a]

Protein	Specific activity (units/mg)	V_{max} (units/mg)	K_m for NAD (mM)	K_m for malate (mM)
Native	700	770	0.30 ± 0.02	1.1 ± 0.1
S226Y	500	550	0.30 ± 0.03	1.3 ± 0.2
D45Y	0.050	0.058	1.22 ± 0.06	12.9 ± 1.0
D45Y/S226Y	0.038	0.042	2.00 ± 0.08	17.7 ± 3.5

[a] MDH activity was determined as described in the Materials and methods section. The error in the measurements as determined by 3 separate experiments is ~3% unless otherwise stated. The protein concentration of the purified protein was determined by a Bio-Rad assay using bovine serum albumin as the standard.

2 categories, which correlated well with their quaternary state. The dimeric S226Y mutant appears to have 70% the activity of the native enzyme and virtually the same K_m for NAD and for malate. The monomeric D45Y mutant has 14,000-fold less activity than the native, with a K_m of 1.22 mM for NAD and 12.9 mM for malate. Both K_m values are higher than the value for the wild-type MDH. The double mutant has a specific activity that is 17,500-fold less than the native with K_m's of 2.00 and 17.7 mM, respectively, for NAD and malate, again more than the native values and even the single mutant monomer. Therefore, the monomeric MDHs have dramatically reduced specific activity and higher K_m values for the coenzyme NAD and the substrate malate.

Crystallographic analysis of mutants

Crystallization trials were done for all 3 mutant forms. The principal reason for these experiments was to show that the modified forms are not denatured. A secondary reason is to utilize X-ray crystallography to determine the 3-dimensional structures of the mutants. Small crystals of all 3 MDH variations have been grown; however, in some instances, mainly thin plate-like or feather-like needle clusters were found. One crystal of the D45Y mutant was suitable for further study and the crystal diffracted to better than 2.8 Å resolution. A complete X-ray data set to 3.1 Å resolution has been recorded and indexed in an orthorhombic lattice. The R_{merge} for the data to 3.1 Å resolution is 11%. A look at the reassembled precession photographs indicated systematic absences along 2 of the principal reciprocal axes. The monomeric MDH therefore crystallized in an orthorhombic $P2_12_12$ space group. The unit cell dimensions are: a = 138.9 Å, b = 155.3 Å, and c = 51.3 Å, and there are 4 monomeric molecules in the asymmetric unit. This crystalline form of the mutant is not isomorphous with the native, and a solution to the phase problem utilizing molecular replacement is under way.

Discussion

In an oligomeric protein such as MDH, the subunit interface should be considered while doing structure-function studies because it may play a subtle role in catalysis. In fact, generally, the number of conserved amino acid residues in the subunit interface of an oligomeric protein is high, pointing toward a possible role in the catalytic mechanism and maintenance of the active-site structure. To fully understand the contributions of subunit interface interactions to the structure and catalytic mechanism, a question that must be asked is whether or not the protomers have activity.

In the case of mMDH, a number of biochemical studies have attempted to sort out the dissociative properties and therefore the relationship of the quaternary structure to enzymatic activity. However, proving the existence of an active monomer has been controversial. Similarly, studies of cMDH have pointed toward a form of cooperativity in the catalytic mechanism that again implies some interaction of the active-site apparatus through the dimer interface (Zimmerle & Alter, 1993).

It is worth noting that the MDHs in general are stable dimers in spite of the pH-sensitive dissociation of mMDH. An assessment of the stability can be crudely obtained by examining the accessible surface area lost upon dimerization. For mMDH, which is highly homologous with eMDH, this value is 13% and amounts to 3,200 Å^2 (Gleason et al., 1994). For eMDH, 3,250 Å^2 are lost upon dimerization, which is 13.5% of the monomer surface area. This is comparable to a variety of stable dimers (Janin et al., 1988). As is generally the case, the stability of the subunit-subunit interface in eMDH is the result of direct hydrogen bonds, water-mediated hydrogen bonds, and hydrophobic contacts.

Crystallographic data and intuition were used to select residues for mutation in eMDH that would interfere with dimer formation. The design of the mutants was based on 3 factors: (1) reducing electrostatic interactions, while simultaneously (2) introducing bad steric contacts, and (3) choosing a residue not involved in catalysis. The last factor would make sure we were only testing the theory that the dimer interface played a role in catalysis, not a particular residue. Two sites were chosen, D45 and S226; both residues were mutated to tyrosines to remove any electrostatic interactions and introduce a large bulky side chain. In the crystallographic model of eMDH, there appears to be no room for a bulky side chain at either of these positions (refer to Fig. 4A,B). One of the 2 predicted sites, D45, correctly produced the desired monomeric form; the other, S226, did not. The double mutant was also a monomer, presumably because of the D45Y mutation.

Construction of the *mdh*$^-$ *E. coli* strain (BHB111) made it possible to easily purify the mutant forms of eMDH. The kinetic data can also be attributed to only the mutant forms of the enzyme because the strain BHB111 has no MDH activity. The lack of activity in the D45Y and D45Y/S226Y mutants is not attributable to lack of folding because the enzymes crystallize and do not behave like a denatured protein on a gel-filtration column.

To illustrate the dimer-to-monomer transition, one can first look at the secondary structure in the interface as is illustrated in Figure 4B and Kinemage 1. This view of the dimer interface shows the 2 pairs of 5 α-helices that are involved in the subunit-subunit interactions: B, C, 2F, 2G, and 3G. Helix B interacts with 3G and with B of the symmetry-related subunit. Helix C fits into a triangular pocket created by the helices 2F, 2G, and 3G, and interacts with the amino-terminus of 2F and the carboxy-terminus of 3G. Especially noteworthy is the fact that helices 2G and 3G have one side in contact with the substrate binding site and the opposite side forming part of the dimer interface. This can be crudely visualized in Figure 4A. The helix,

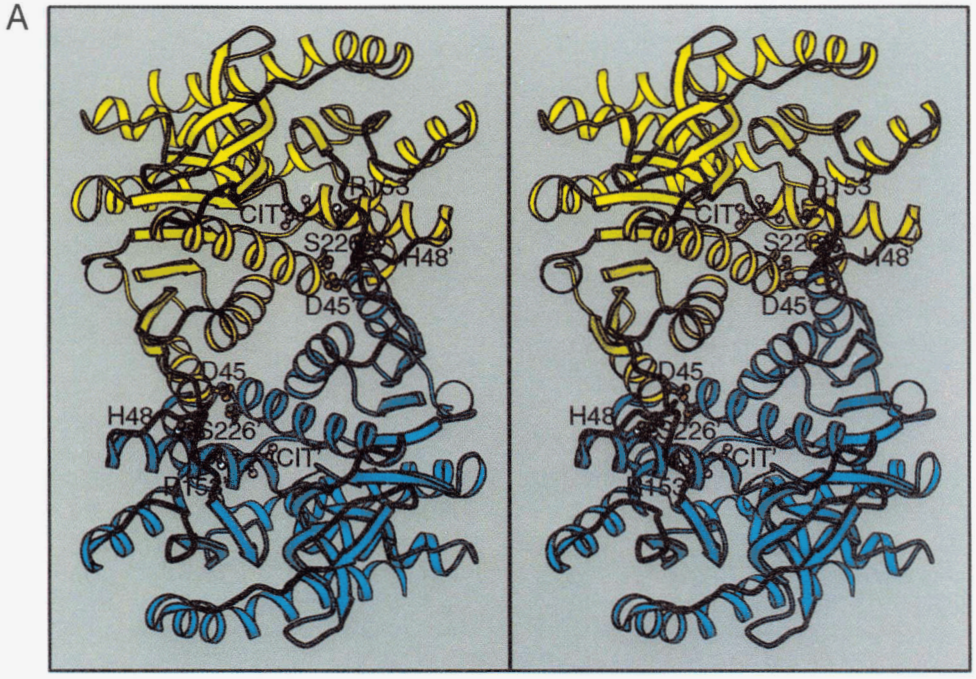

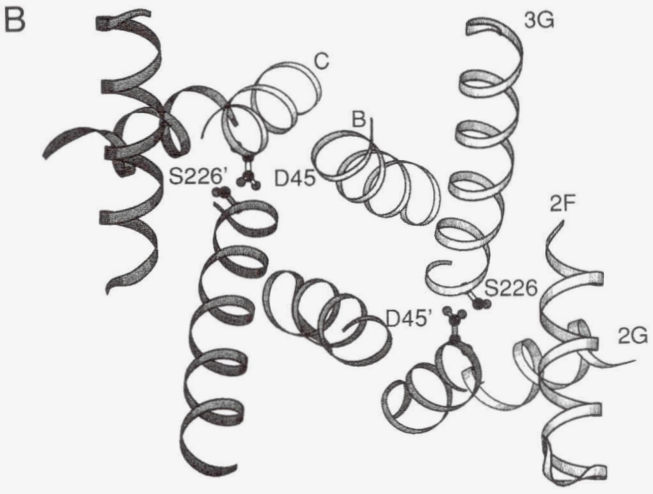

Fig. 4. Ribbon diagram of the MDH dimer interface. **A:** The stereodiagram illustrates the overall organization of the subunits in the MDH dimer. Subunit I is in orange and yellow with subunit II in 2 shades of blue. The orange and darker blue colors designate the region of the dimer interface described more completely in Figure 4B. The 2 mutations, D45 and S226 are labeled for both subunits (subunit II contains the primed residues), along with H48 and R153. H48 is hydrogen bonded across the dimer interface to R153, 1 of the 3 arginines that bind the substrate. The location of the dicarboxylic acid binding site is indicated by the analogue—citrate. The letters "CIT" are used to label this site with the citrate found in pink. **B:** The diagram contains a ribbon representation of the 5 α-helices that form the dimer interface, drawn with MOLSCRIPT (Kraulis, 1991). The α-helices are drawn as ribbon spirals and are labeled according to the convention for MDHs. The α-helices for one subunit are darker than for the other. The mutated residues are also labeled in the diagram, one subunit having D45 and S226 and the other D45′ and S226′. The helices are labeled according to their appearance in the primary structure (Rossmann et al., 1975). Helices B and C are in the nucleotide binding domain (residues 1–150). Helix 2F is near the connection and 2G and 3G are in the catalytic domain.

3G, includes residue S226 and the active site is indicated by the location of the substrate analogue—citrate (labeled CIT).

The positions of the 2 mutated residues are also illustrated in Figure 4A and B and Kinemage 1, D45 on helix C, and S226 on 3G in the dimer interface. D45 is pointing directly into the amino-terminal end of the helix 3G of the symmetry-related subunit. Each of the oxygens of the D45 side chain forms hydrogen bonds to main-chain nitrogen atoms of the other subunit, one to T224, the other to S226 (Fig. 5B). In addition, the 2 side-chain oxygens of D45 form hydrogen bonds with the side-chain —OHs of the same 2 residues in the symmetry-related subunits. D45 is therefore, in a very unusual location interacting with the N-terminal main-chain atoms of an α-helix and the side chains of the same 2 residues. In other terms, the negative charge of D45 is positioned nearly optimally to interact with the positive end of the helical dipole belonging to 3G.

The crystallographic model therefore helps to explain the observed dimer-to-monomer transition; the change is due to alterations in the electrostatic interactions between D45 and the end of an α-helix in the symmetry-related subunit and the introduction of a large bulky side chain for which there is no room. The measurements of the enzymatic activity described in the Results section show that the formation of monomeric enzyme greatly reduces the catalytic capability. We are confident the D45Y alteration could not be affecting the active site in the same subunit. The distance from D45 to the active site in its own subunit is greater than 20 Å and there is no obvious electrostatic network connecting the 2 regions. The loss of activity must therefore be the result of the loss of the subunit interface accompanying the formation of monomeric enzyme.

The K_m for NAD between the dimeric and monomeric forms changed somewhat, but not dramatically, agreeing with the crys-

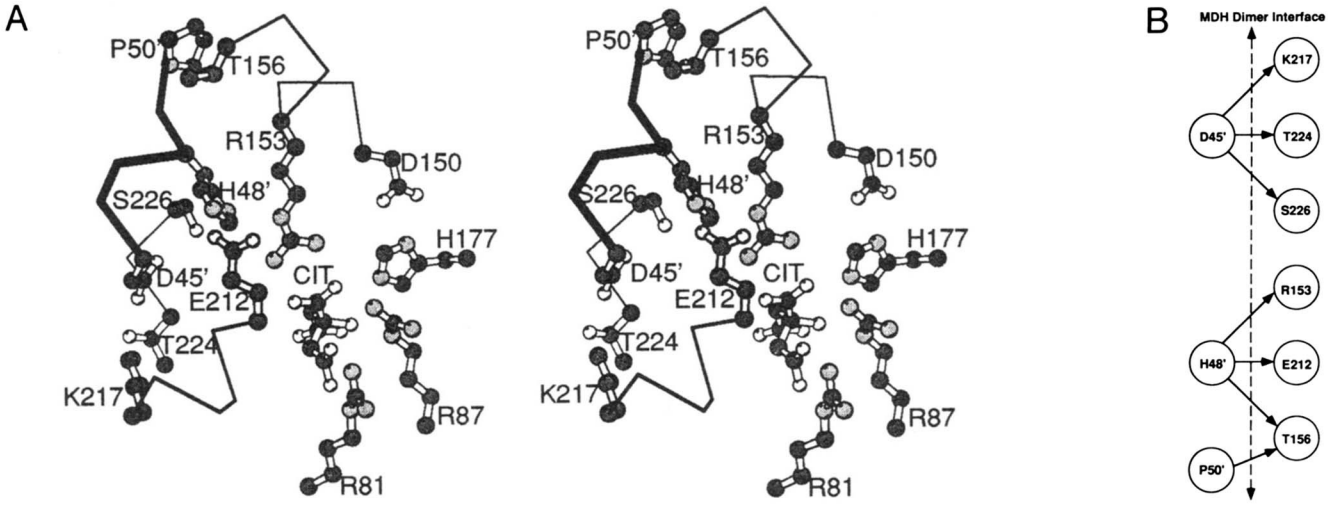

Fig. 5. The subunit–subunit interface and active site of eMDH. **A:** The stereo view contains the residues within hydrogen bonding distance in the dimer interface and involved in substrate binding. The substrate analog is citrate and can be seen in the lower right quadrant of the diagram. The proton relay system can be seen on the right side of the diagram (D150 and H177). The H48′ of the dark subunit is within hydrogen bonding distance of R153, one of residues that binds the citrate in the active site of eMDH. The hydrogen bonding pattern is seen in the figure below. Carbon atoms are depicted as black, nitrogen as gray, and oxygen atoms are white. **B:** Schematic representation of the key residues in the subunit–subunit interface. The residues to the left of the dotted line include D45′, which was mutated to a tyrosine. To the right of the dotted line are shown the complementary side chains of the other subunit. Among them, R153 is responsible for binding the substrate; note that it interacts with H48′ of the symmetry-related subunit.

tallographic observation that the coenzyme binding site is not near the segment of the interface near D45. In fact, D45 is minimally 8 Å from the closest atom in the nicotinamide ring and 20 Å or more from atoms in the adenine ring of the bound coenzyme.

Again, the best explanation would place emphasis on the loss of the subunit interface not a direct electrostatic effect. As seen in Figure 5A and Kinemage 2 (and also Fig. 4A), arginine 153 is responsible for interacting with the carboxylate of the substrate in both the MDHs and the LDHs. It is conserved throughout all the structures. In eMDH, H48 hydrogen bonds to R153 across the subunit interface. This must lock the side chain of R153 into the optimal binding position for the substrate. Because the same arginine is present in both the MDHs and the LDHs, we would predict that a monomeric form of either the LDHs or the MDHs will have dramatically reduced activity. In the absence of the interface and H48, R153 is probably not positioned correctly for substrate binding and the turnover number will be reduced dramatically. Not unexpectedly, the K_m for malate for the monomeric forms of MDH is more than 10 times that of the dimeric forms.

Last of all, it is worth asking why the S226Y mutant did not lead to a monomeric form of the enzyme. This observation suggests that a tyrosine at position 226 can be accommodated at the tight interface. The mutation is electrostatically neutral at most pHs and if the bulkier tyrosine side chain can be accommodated by a different rotamer position, the enzyme remains a dimer. Also, S226 is only 1 of the 3 residues within hydrogen bonding distance of D45 (Fig. 5B), which still has 2 other viable hydrogen bonds to keep the dimer interface intact.

It is also interesting to speculate about the possibility of second-site revertants, other mutations to bring back the enzymatic activity of the monomeric form. An analysis of the crystal structure of eMDH suggests that this will be very difficult to accomplish. In the absence of the other subunit, especially residue H48, it appears that R153 could occupy a position on the surface of the monomeric enzyme. We estimate that without disturbing the main-chain conformation, the new position in the solvent would be at the former site of H48 in the opposing subunit. This is minimally 4 Å from the active-site location. It is not clear how one could constrain the position of R153 in the absence of the dimer interface. It appears therefore, that monomeric forms of malate/lactate-type dehydrogenases are doomed to being poor catalysts.

The characterization of the monomeric mutant of eMDH shows that a relatively small change at a key residue can disrupt the extensive subunit–subunit interactions. It also helps to clarify the role the dimer interface plays in the catalytic function. The specific activity of the altered enzymes was dependent on its oligomeric state. The dimeric mutant, S226Y, gave only small decreases in the specific activity. However, the monomeric D45Y enzyme had a specific activity that was dramatically decreased. In conclusion, the data presented here provide evidence for a catalytic mechanism that is largely dependent on the dimeric structure of the enzyme.

Materials and methods

Construction of BHB111, an mdh⁻ strain of E. coli

An *E. coli* strain that does not produce MDH was constructed in order to simplify purification of the mutant forms of eMDH. Originally, a Tn*10* gene (Tet^R) from CAG12071 was introduced upstream of the *mdh* gene in strain DV21A05, to produce our starting Hfr donor strain DE130. To produce a null mutation in the wild-type *mdh* gene in the chromosome of DE130, we re-

placed these sequences with a disrupted *mdh* gene carried by the plasmid pED7 (Fig. 2). This plasmid was constructed by insertion of a Kan-resistant gene into the *mdh* sequences of the plasmid pRV7 (Vogel et al., 1987). This plasmid also contains an Amp^R marker.

Briefly, pRV7 was partially cut with *Pvu*II and the *kan* cassette was inserted at the *Pvu*II site roughly in the middle of the *mdh* gene. The disrupted sequences were then transferred to the chromosome using the technique described by Resnik and LaPorte (1991). pED7 was transformed into an Hfr strain (DE130) having a wild-type copy of *mdh* and a Tn*10* gene, near the point of origin of transfer. The *mdh* sequences flanking the *kan* gene allowed homologous recombination with the wild-type *mdh* gene in the chromosome. Transfer of these sequences by conjugation with W4680 increased the recovery of the desired recombination products, which is otherwise a low frequency event. Exconjugates were selected for Tet^R, $Strep^R$, and Amp^R to ensure the transfer of the plasmid into the recipient strain. To get rid of the plasmid, which after recombination would contain the wild-type *mdh* sequences, a P1 transduction from the exconjugates into W4680 was performed to transfer only chromosomal sequences. After the final transduction, the new strain (BHB111) carries a *kan* gene in the middle of the *mdh* gene, a Tn*10* gene nearby, and $Strep^R$ given to it by the parent W4680; however, it should be Amp^S because it is not carrying a plasmid.

The doubling time of the mutant strain (BHB111) versus the wild-type parent strain (W4680) was determined by growth in MOPS-minimal media plus either 1% acetate or glucose. Also, the activity of the crude extract of BHB111, W4680, and BHB111 with the wild-type plasmid was determined. The protocol was as follows. The mutant and wild-type strains were grown on LB media at 37 °C until an OD_{600} of about 1.5 was reached. BHB111 with the plasmid carrying the wild-type *mdh* gene was grown similarly with no induction, as a control. The cells were spun down, resuspended in cracking buffer containing 50 mM Tris, pH 7.9, 10% sucrose, 0.05% NaN_3, 1 mM EDTA, and 2 mM DTT, and disrupted by sonication. The cell lysate was then centrifuged for 30 min at 17,000 rpm to remove cell debris. A 0.4% PEI precipitation was done to remove DNA, and the suspension was centrifuged for 30 min at 17,000 rpm. The supernatant was then used for enzyme activity assays. The frequency of cotransduction of the Tet^R and Kan^R markers was also determined by P1 transduction. P1 lysates of BHB111 were produced and subcloned into W4680. The cells were then plated first on Kan plates and then on Tet plates and vice versa. To determine the distance between markers the equation $F = (1 - D/L)^3$ was used, where F is the frequency of cotransduction, D is the distance between markers, and L is the length of DNA packaged by the P1 virion.

Site-directed mutagenesis

Site-directed mutants of MDH isolated from *E. coli* were produced following the Muta-Gene Phagemid in vitro mutagenesis protocol from Bio-Rad. A *Bam*HI-*Sph*I fragment of pRV7 containing the wild-type *mdh* gene was subcloned into the same sites in the phagemids, pT7/T3α-18 and pT7/T3α-19, producing MBBα-18 and MBBα-19. The mutagenesis was accomplished by hybridizing a synthetic oligonucleotide, with the proposed mismatch in the center, to single-stranded wild-type DNA from MBBα-18 with uracils incorporated. The oligonucleotide primers changed the 3-base codon, in both instances, to a TAT from GAT, in the D45Y case, or TCT in the S226Y case. The 2 complementary oligonucleotides are shown with the mismatch in parentheses: D45Y = 5′ ATG GCT CAG (A)TA GAC AGC CAC AC and S226Y = 5′ CTG GCC CAT A(T)A CAG GGT TGC AGA. After hybridization, the synthetic oligonucleotides were extended with cloned *Pfu* DNA polymerase and the nick was sealed with DNA ligase.

This double-stranded plasmid was then transformed into the mdh^- *E. coli* host (BHB111), which has an active uracil-*N*-glycosylase that inactivates the uracil-containing strand. The transformation was then plated on LB-Amp plates. Theoretically, only the mutant strand then replicates. To check whether mutagenesis was successful, the DNA was sequenced using an ABI sequencer. The sequencing reactions were prepared using the PRISM Ready Reaction DyeDeoxy Terminator Cycle Sequencing kit. Three colonies were picked for sequencing each mutant constructed, and all 3 contained the mutation. Three mutants have been produced, D45Y, S226Y, and the double mutant D45Y/S226Y. The plasmids that contain the mutated eMDHs are labeled MBBα-18(D45Y), MBBα-18(S226Y), and MBBα-18(D45Y/S226Y).

Purification and analysis of mutant enzymes

The mutant enzymes purified in this study came from the 3 plasmid sources pMBBα-18(D45Y) or (S226Y) or (D45Y/S226Y) transformed into the *E. coli* strain BHB111. The mutagenesis vector was also used for expression of the mutant proteins. Cells were grown in LB-based fermentor media and 200–300 mg/L amp in a 3.5-L high-density fermentor. They were induced with 1–2 mM IPTG in mid-log phase and grown for another 3–4 h. The cells were harvested by centrifugation and stored in the freezer at −80 °C.

At the start of the purification scheme, cells were thawed and resuspended in cracking buffer containing 50 mM Tris, pH 7.9, 10% sucrose, 0.05% NaN_3, 1 mM EDTA, and 2 mM DTT. The cells were then disrupted by sonication, 7–8 times for 1-min intervals. The cell lysate was then centrifuged for 1 h at 17,000 rpm to remove cell debris. A 0.4% PEI precipitation was done to remove DNA, and the lysate was centrifuged for 45 min at 17,000 rpm. A 75% ammonium sulfate precipitate was performed on the PEI supernatant to remove unwanted proteins and concentrate the MDH. The pellet was stored in the −80 °C freezer.

The pellet was resuspended in buffer containing 20 mM Tris-HCl, pH 8.5, 2 mM EDTA, 2 mM DTT, 0.05% NaN_3, and dialyzed versus the buffer overnight with 2 buffer changes. The dialysate was loaded onto a Q-sepharose column previously equilibrated with the starting buffer. A salt gradient consisting of 0–0.5 M NaCl was applied to the column. Most of the MDH was found in the initial breakthrough fractions by activity assays and was nearly pure, as assessed by SDS/PAGE gels. The MDH from the Q-sepharose column was pooled, concentrated and dialyzed overnight versus 20 mM Hepes, pH 7.4, 2 mM EDTA, 2 mM DTT, 0.05% NaN_3. This fraction was then loaded on a Blue Sepharose column. The MDH was eluted with a 900-mL salt gradient, 0–0.5 M NaCl. Those fractions containing only eMDH were pooled and concentrated to about 10–12 mg/mL, then split into 2 pools; one was dialyzed versus water for crystallization trials and the other was dialyzed versus 50 mM Tris-HCl, pH 7.6, 5 mM EDTA, 5 mM DTT, 0.05% NaN_3 for later use in the kinetic experiments.

All gels were run on a Pharmacia PhastSystem with the SDS-PAGE and native-PAGE gels being 20% homogeneous polyacrylamide gels with a stacking zone of 7.5% total acrylamide and 3.0% crosslinked acrylamide and a separation zone of 20% T and 2% C. The SDS gels were run under denaturing conditions and the native gels were run under native conditions. The IEF gels were 5% T and 3% C. The concentration of the enzyme was determined versus BSA with the Bio-Rad protein assay.

Gel-filtration chromatography for molecular weight determination was performed using a Sephadex G-200 column (1.6 × 53 cm). The column was equilibrated with 20 mM Tris-HCl, pH 7.4, 40 mM KCl, 0.05% NaN_3 at 4 °C. The column was run at 0.2 mL/min. Appropriate proteins of known molecular weight were used to calibrate the column. Protein elution was monitored at 280 nm with an LKB Bromma 2141 Variable Wavelength Monitor connected to a Pharmacia FPLC. The molecular weights of the unknowns, native, and mutant MDH were determined from their elution volumes.

MDH assay/steady-state kinetics

MDH activity is assayed by measuring the increase in NADH absorbance at 340 nm accompanying the conversion of malate to oxaloacetate. The assay was carried out in a 1-mL cuvette with 940 μL of the assay buffer (840 μL of 0.1 M sodium glycinate, pH 10.0; 100 μL of 1.0 M malic acid, pH 7.0), and 50 μL of 50 mM NAD (2.5 mM) for the native and S226Y enzyme, or 50 μL of 120 mM NAD (6 mM) in the D45Y and D45Y/S226Y cases. The spectrophotometer was zeroed at 340 nm and the reaction was initiated with 10 μL of appropriately diluted enzyme. The temperature of the cuvette was maintained at 25 °C by a circulating water bath.

A series of steady-state kinetic analyses were carried out to determine the K_m's for both NAD and malate for the native and mutant enzymes. In the case of the native and S226Y enzyme, bovine serum albumin (1 mg/mL) was added to protect the enzyme against inactivation at low concentration. The concentration of NAD was varied between 0.125 and 2.5 mM for the native and S226Y mutant and between 0.188 and 12 mM for the D45Y and double mutant. The concentration of malate was varied between 0.5 and 10.0 mM for the native and S226Y mutant and between 1.0 and 100.0 mM for the D45Y and double mutant. The program ENZFITTER (Leatherbarrow, 1987) was used for the calculation of K_m and its standard deviations.

Crystallization

Crystals of all 3 mutants have been grown using the hanging drop vapor diffusion method at room temperature. A 10-μL drop containing 5 μL of protein solution (7–9 mg/mL) and 5 μL of the crystallization buffer was suspended on a silanized cover slip over 1 mL of buffer. The D45Y and D45Y/S226Y crystals grow in Na-citrate, pH 5.5, with 20% PEG_{8000}, 200 mM MgAc, 1 mM DTT, and 1 mM EDTA. The S226Y crystals grow in Na-citrate, pH 5.5, with 200 mM $LiSO_4$ or in Tris buffer with 200 mM Na-tartrate, with either 20% PEG_{8000} or 30% PEG_{4000}, plus DTT and EDTA. These conditions have not been completely optimized, however, 1 D45Y crystal did grow large enough to collect data. The crystal was mounted in a glass capillary tube and data were collected on a Siemens-Nicollet area detector, with a Rigaku rotating anode X-ray generator running at 50 kV and 200 mA. Fifty frames of data were collected with a $2\theta = 0°$ in order to do the initial indexing and determine if the crystal would be useful for data collection. Subsequent data runs were done with $2\theta = -13°$. All data processing was done with the Xengen package and the data were initially processed in the primitive lattice to determine the space group and unit cell dimensions. The program HKLVIEW from CCP4 was used to look at pseudo-precession photographs.

Acknowledgments

We are grateful for the advice and guidance of Dr. David LaPorte in the construction of the *mdh*⁻ strain of *E. coli*. We acknowledge the contributions of Ed Hoeffner, who maintains both the X-ray and computing resources used during this study. We thank Dr. Michael Hall, who was instrumental in the initial mutant design stage. Thanks also go to Lael Melchert and Kevin Albers for help with the kinetic studies. The studies were supported by a grant (MCB9318699) from the NSF. D.B. is grateful to the NIH for a postdoctoral fellowship (1 F32 GM15663-01).

References

Birktoft JJ, Rhodes G, Banaszak LJ. 1989. Refined crystal structure of cytoplasmic malate dehydrogenase at 2.5 Å resolution. *Biochemistry 28*:6065–6081.

Bleile DM, Schulz RA, Gregory EM, Harrison JH. 1977. Investigation of the subunit interactions in malate dehydrogenase. *J Biol Chem 252*: 755–758.

Borchert TV, Abagyan R, Radha Kishan KV, Zeelen JPh, Wierenga RK. 1993. The crystal structure of an engineered monomeric triosephosphate isomerase, monoTIM: The correct modelling of an eight-residue loop. *Structure 1*:205–231.

DuVal G, Swaisgood HE, Horton HR. 1985. Some kinetic characteristics of immobilized protomers and native dimers of mitochondrial malate dehydrogenase: An examination of the enzyme mechanism. *Biochemistry 24*:2067–2072.

Gleason W, Fu Z, Birktoft J, Banaszak L. 1994. Refined crystal structure of mitochondrial malate dehydrogenase from porcine heart and the consensus structure for dicarboxylic acid oxidoreductases. *Biochemistry 33*:2078–2088.

Hall MD, Levitt DG, Banaszak LJ. 1992. The crystal structure of *E. coli* malate dehydrogenase: A complex of the apoenzyme and citrate at 1.9 Å resolution. *J Mol Biol 226*:867–882.

Harada K, Wolfe RG. 1968. Malic dehydrogenase: The catalytic mechanism and possible role of identical protein subunits. *J Biol Chem 243*:4131–4137.

Honka E, Fabry S, Niermann T, Palm P, Hensel R. 1990. Properties and primary sequence of the L-malate dehydrogenase for the extremely thermophilic archaebacterium *Methanothermus fervidus*. *Eur J Biochem 188*:623–632.

Jackson RM, Gelpi J, Cortes A, Emery D, Wilks H, Moreton K, Halsall D, Sleigh R, Behan-Martin M, Jones G, Clarke A, Holbrook J. 1992. Construction of a stable dimer of *Bacillus stearothermophilus* lactate dehydrogenase. *Biochemistry 31*:8307–8314.

Janin J, Miller S, Chothia C. 1988. Surface, subunit interfaces and interior of oligomeric proteins. *J Mol Biol 204*:155–164.

Jurgensen SR, Harrison JH. 1982. Active subunits in hybrid-modified malate dehydrogenase. *J Biol Chem 257*:569–574.

Jurgensen SR, Wood DC, Mahler JC, Harrison JH. 1981. The immobilization of mitochondrial malate dehydrogenase on sepharose beads and the demonstration of catalytically active subunits. *J Biol Chem 256*: 2383–2388.

Kelly CA, Nishiyama M, Ohnishi Y, Beppu T, Birktoft JJ. 1993. Determinants of protein thermostability observed in the 1.9 Å crystal structure of malate dehydrogenase from the thermophilic bacterium *Thermus flavus*. *Biochemistry 32*:3913–3922.

Kraulis P. 1991. MOLSCRIPT: A program to produce both detailed and schematic plots of proteins. *J Appl Crystallogr 24*:946–950.

Leatherbarrow RJ. 1987. *ENZFITTER manual: A non-linear regression data analysis program for the IBM PC (and true compatibles)*. Cambridge, UK: BIOSOFT.

McEvily AJ, Mullinax TR, Dulin DR, Harrison JH. 1985. Regulation of mitochondrial malate dehydrogenase: Kinetic modulation independent of subunit interaction. *Arch Biochem Biophys 238*:229–236.

Mullinax TR, Mock JN, McEvily AJ, Harrison JH. 1982. Regulation of mitochondrial malate dehydrogenase: Evidence for an allosteric citrate-binding site. *J Biol Chem 257*:13233–13239.

Resnik E, LaPorte DC. 1991. Introduction of the single-copy sequences in the chromosome of *Escherichia coli*: Application to gene and operon fusions. *Gene 107*:19–25.

Roderick SL, Banaszak LJ. 1986. The three-dimensional structure of porcine heart mitochondrial malate dehydrogenase at 3.0 Å resolution. *J Biol Chem 261*:9461–9464.

Rossmann MG, Liljas A, Branden CI, Banaszak LJ. 1975. Evolutionary and structural relationships among dehydrogenases. In: Boyer PD, ed. *The enzymes*. New York: Academic Press. pp 61–102.

Steffan JS, McAlister-Henn L. 1991. Structural and functional effects of mutations altering the subunit interface of mitochondrial malate dehydrogenase. *Arch Biochem Biophys 2*:276–282.

Vogel RF, Entian KD, Mecke D. 1987. Cloning and sequence of the *mdh* structural gene of *Escherichia coli* coding for malate dehydrogenase. *Arch Microbiol 149*:36–42.

Wood DC, Hodges CT, Howell SM, Clary LG, Harrison JH. 1981a. The *N*-ethylmaleimide-sensitive cysteine residue in the pH-dependent subunit interactions of malate dehydrogenase. *J Biol Chem 256*:9895–9900.

Wood DC, Jurgensen SR, Geesin JC, Harrison JH. 1981b. Subunit interactions in mitochondrial malate dehydrogenase: Kinetics and mechanism of reassociation. *J Biol Chem 256*:2377–2382.

Zimmerle C, Alter G. 1993. Cooperativity in the mechanism of malate dehydrogenase. *Biochemistry 32*:1274–12748.